In Vivo Imaging of Human Acetylcholinesterase Density in Peripheral Organs Using ^{11}C-Donepezil: Dosimetry, Biodistribution, and Kinetic Analyses

Trine Gjerløff[1], Steen Jakobsen[1], Adjmal Nahimi[1], Ole L. Munk[1], Dirk Bender[1], Aage K.O. Alstrup[1], Karina H. Vase[1], Søren B. Hansen[1], David J. Brooks[1,2], and Per Borghammer[1]

[1]Department of Nuclear Medicine and PET Centre, Aarhus University Hospital, Aarhus, Denmark; and [2]Department of Medicine, Imperial College London, London, United Kingdom

Brain cholinergic function has been previously studied with PET but little effort has been devoted to imaging peripheral organs. Many disorders, including diabetes and Parkinson disease, are associated with autonomic dysfunction including parasympathetic denervation. Nonneuronal cholinergic signaling is also involved in immune responses to infections and in cancer pathogenesis. 5-^{11}C-methoxy-donepezil, a noncompetitive acetylcholinesterase ligand, was previously validated for imaging cerebral levels of acetylcholinesterase. In the present study, we explored the utility of ^{11}C-donepezil for imaging acetylcholinesterase densities in peripheral organs, including the salivary glands, heart, stomach, intestine, pancreas, liver, and spleen. **Methods:** With autoradiography, we determined binding affinities and levels of nonspecific ^{11}C-donepezil binding to porcine tissues. Radiation dosimetry was estimated by whole-body PET of a single human volunteer. Biodistribution and kinetic analyses of ^{11}C-donepezil time–activity curves were assessed with dynamic PET scans of 6 healthy human volunteers. A single pig with bacterial abscesses was PET-scanned to explore ^{11}C-donepezil uptake in infections. **Results:** Autoradiography showed high ^{11}C-donepezil binding (dissociation constant, 6–39 nM) in pig peripheral organs with low nonspecific signal. Radiation dosimetry was favorable (effective dose, 5.2 μSv/MBq). Peripheral metabolization of ^{11}C-donepezil was low (>90% unchanged ligand at 60 min). Slow washout kinetics were seen in the salivary glands, heart, intestines, pancreas, and prostate. A linear correlation was seen between ^{11}C-donepezil volumes of distribution and standardized uptake values, suggesting that arterial blood sampling may not be necessary for modeling uptake kinetics in future ^{11}C-donepezil PET studies. High standardized uptake values and slow washout kinetics were seen in bacterial abscesses. **Conclusion:** ^{11}C-donepezil PET is suitable for imaging acetylcholinesterase densities in peripheral organs. Its uptake may potentially be quantitated with static whole-body PET scans not requiring arterial blood sampling. We also demonstrated high ^{11}C-donepezil binding in bacterial abscesses. We propose that ^{11}C-donepezil PET imaging may be able to quantify the parasympathetic innervation of organs but also detect nonneuronal cholinergic activity in infections.

The enzyme acetylcholinesterase is situated in the synaptic cleft of cholinergic synapses. Acetylcholinesterase breaks down acetylcholine and thereby terminates cholinergic neurotransmission. Cerebral acetylcholinesterase function has been thoroughly studied with PET (1).

To our knowledge, no PET studies have attempted to quantify the activity or density of acetylcholinesterase in peripheral organs in different disease states. Although acetylcholinesterase is not exclusively produced by cholinergic neurons, histologic measurements of acetylcholinesterase activity have been used for decades to quantify cholinergic terminal function of parasympathetic, enteric, and cardiac innervation (2,3). Early studies reported that subdiaphragmatic vagotomy induces a 50% decrease of acetylcholinesterase activity in the gastrointestinal tract of guinea pigs (2). This finding suggests that acetylcholinesterase imaging provides a marker of parasympathetic innervation, known to be damaged in diabetes and Parkinson disease (4).

Recently, there has been increasing interest in nonneuronal cholinergic transmission, which plays an important role in regulation of immune function. Peripheral lymphocytes express choline acetyltransferase, vesicular acetylcholine transporters, acetylcholinesterase, and muscarinergic receptors (5). Several of these components, including acetylcholinesterase, are upregulated in activated lymphocytes (5). Cholinergic imaging may therefore provide a marker of immune activity in infections and inflammation.

Previous PET studies of acetylcholinesterase have used substrate-like radioligands. These ligands, such as ^{11}C-N-methyl-4-piperidyl acetate (^{11}C-MP4A) (6), are analogs of acetylcholine, the primary substrate of acetylcholinesterase. Unlike acetylcholine, ^{11}C-MP4A (a lipophilic tertiary amine structure) can cross the blood–brain barrier. Once inside the brain, it is hydrolyzed by acetylcholinesterase, forming the hydrophilic radioactive metabolite N-^{11}C-methyl-4-piperidinol, which is retained in the brain because of its low blood–brain barrier permeability. However, in peripheral organs there is no trapping of N-^{11}C-methyl-4-piperidinol, preventing the use of ^{11}C-MP4A PET imaging outside the brain.

Recently, 5-^{11}C-methoxy-donepezil has been successfully used to visualize decreased acetylcholinesterase density in the brains of
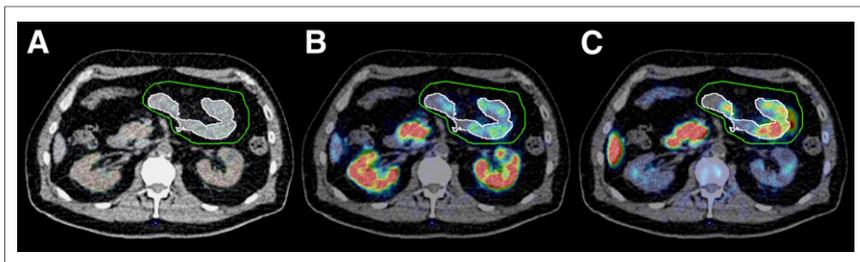
FIGURE 1. (A) Large PET VOI (green outline) included all radioactivity from intestines and stomach, respectively. To derive volume estimate, a VOI was segmented based on CT scan (white outline). (B) During early PET frames, radioactivity corresponded to anatomic outline. (C) At later PET frames, PET signal was displaced due to peristalsis but was included in large PET VOI.

patients with Alzheimer or Parkinson disease (7,8). Donepezil is a standard pharmacologic treatment of patients with Alzheimer disease (9) and a noncompetitive, high-affinity, reversible antagonist of acetylcholinesterase. Furthermore, donepezil has a high degree of selectivity for acetylcholinesterase over butyrylcholinesterase. Hence,[11]C-donepezil is a ligand-type radioprobe and could have a favorable pharmacokinetic profile for imaging acetylcholinesterase densities in peripheral organs. Importantly, little peripheral ^{11}C-donepezil metabolism occurs during a 60-min PET scan, potentially removing the need for metabolite correction (10). ^{11}C-donepezil PET could therefore be a suitable tool for imaging neuronal and nonneuronal cholinergic mechanisms in peripheral organs.

The goals of the present study were to assess radiation dosimetry and the biodistribution of ^{11}C-donepezil in healthy human volunteers and to perform kinetic analyses of its uptake. Using ^{11}C-donepezil autoradiography, we also investigated the binding affinity and level of nonspecific binding of various porcine tissues. Finally, a single pig with bacterial abscesses was scanned to evaluate the ability of ^{11}C-donepezil PET to image cholinergic signaling in infections.

MATERIALS AND METHODS

Preparation of ^{11}C-Donepezil

A detailed description of the ^{11}C-donepezil synthetic route is provided in the supplemental materials (available at http://jnm.snmjournals.org). Briefly, cyclotron-derived ^{11}C-carbon was converted to ^{11}C-methyliodide, which was trapped in dimethyl sulfoxid (300 μL) containing NaOH (1 μL, 2 mol/L) and 5-O-desmethyl donepezil (0.5 mg). The mixture was heated at 80°C for 5 min. Purification of ^{11}C-donepezil was performed by high-performance liquid chromatography.

In Vitro Autoradiography

Postmortem tissue samples were obtained from female Danish Landrace pigs (3 mo, 40 kg). The study was approved by the Danish Animal Experiments Inspectorate. The postmortem interval until freezing was less than 30 min. The following tissues were investigated: myocardium ($n = 5$ pigs), stomach wall ($n = 3$), intestines ($n = 3$), pancreas ($n = 2$), spleen ($n = 2$), salivary gland ($n = 2$), kidney ($n = 1$), and brain ($n = 1$). Samples were flash-frozen at $-30°C$ using dry ice and isopentane and transferred to a $-80°C$ freezer for storage.

Each tissue block was cut into 20-μm sections at $-20°C$ using a freezing sliding microtome and thaw-mounted on polylysine-coated slides. Before autoradiography, sections were warmed to room temperature, dried, and preincubated in phosphate-buffered saline (pH 7.4) for 20 min. Displacement studies were performed by incubating ^{11}C-donepezil (40 MBq/L; specific activity, 129–170 GBq/μmol) in the same buffer at temperature 20°C for 20 min in the presence of the following concentrations of cold donepezil: 0 nM, 1 nM, 10 nM, 100 nM,

and 10 μM. Hot ligand concentration was 0.03–0.06 nM during incubation. Sections were then dipped 3 times in cold, distilled water and dried under a cool-air stream. Slides were exposed on imaging plates in an autoradiographic cassette for 2 h and developed using BAS-MS 2025 (Fujifilm). Autoradiography slides were subsequently stained with hematoxylin and eosin for histologic inspection.

The digital autoradiograms were analyzed using Image Gauge 4.0 (Fujifilm). Regions of interest were drawn in gastrointestinal mucosa, parenchyma of pancreas, spleen, salivary glands, kidney cortex, myocardium, and brain gray matter, and representative background regions of interest were drawn on each slide. We used the homogeneous self-competition study analysis in Prism 6 (GraphPad Software) to estimate the dissociation constant (K_d) with the simplified Cheng–Prusoff equation (11): K_d = half maximal inhibitory concentration – [L]. A single-site model of binding was assumed.

Human Study Population

A healthy 64-y-old male volunteer was recruited for a whole-body ^{11}C-donepezil dosimetry PET study. Tracer biodistribution, kinetics, and blood metabolism were studied in 6 healthy male subjects (mean age ± SD, 64.7 ± 6.3 y). Exclusion criteria included systemic diseases, cancer, previous irradiation to the head and neck, previous major surgery to the gastrointestinal tract, neurologic disease, psychiatric disease, and substance abuse disorders. No subjects received anticoagulant treatment or medications affecting cholinergic signaling.

The study protocol was approved by the Central Denmark Region Committee on Health Research and by the Danish Health and Medicines Authority. All subjects signed a written informed consent form. The study was registered in the www.clinicaltrials.gov database (NCT01877538). Subjects were screened in the morning on the day of PET. Screening included recording of demographic data, clinical history, medication, medical and neurologic examination, heart rate, and blood pressure measurements before and after PET. All participants were fasting, for a minimum of 8 h from solid foods and 4 h from liquids, on the day of PET.

Whole-Body PET Imaging

Pseudodynamic whole-body PET was performed on a healthy male volunteer using a Biograph PET/CT camera (Siemens AG) operated in 3-dimensional mode. Immediately before PET, we performed low-dose CT, from the vertex to the mid thigh. The imaging field of view was 21.8 cm. Two minutes before the scan start, 395 MBq of ^{11}C-donepezil were injected as a bolus. Five consecutive whole-body scans were obtained with increasing frame durations: 1, 1.5, 2, 2.5, and 3 min per bed position. Thus, 5 emission recordings were performed during the following time intervals: 2–7, 8–16, 17–28, 29–44, and 45–62 min. Twelve source organs were used in the dosimetry calculation: liver, spleen, bone marrow, brain, thyroid, heart wall, adrenals, pancreas, kidneys, stomach, small intestine, and bladder. Organ doses and the effective dose were calculated using the OLINDA software package (12) based on the MIRD method.

Dynamic PET Imaging

Two catheters were inserted: 1 in the radial artery for blood sampling and 1 in the opposite anterior cubital vein for injection of ^{11}C-donepezil. For each of the 6 subjects, two 60-min dynamic PET scans separated by a 70-min break were obtained. For both scans, the subjects were placed supine. ^{11}C-donepezil was injected as a standardized 60-s bolus using a NE-500 OEM syringe pump (New Era Pump Systems). During
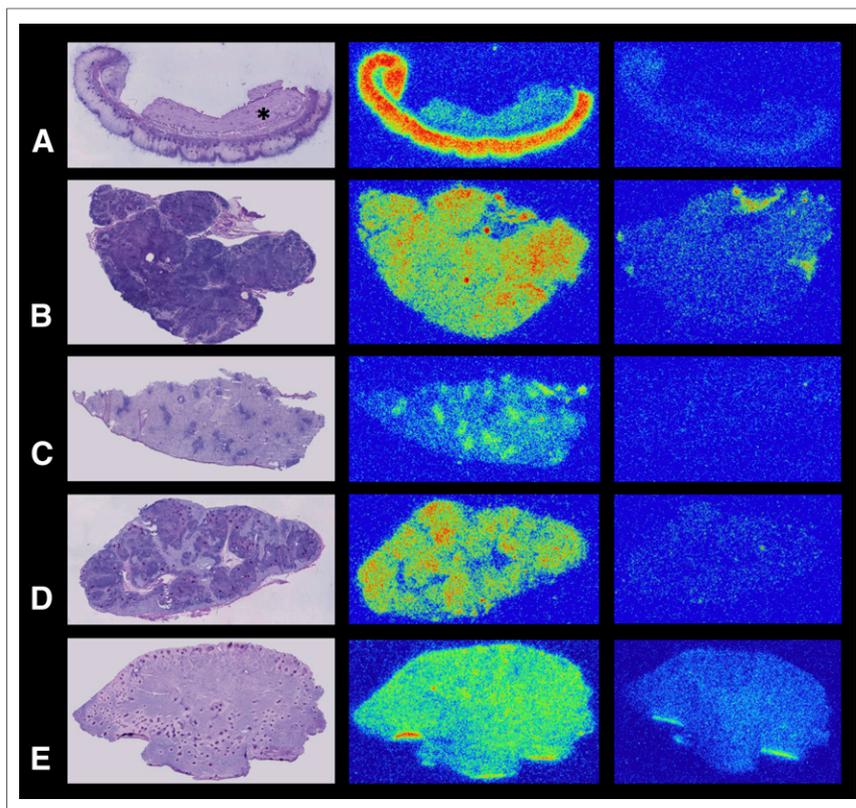
FIGURE 2. ¹¹C-donepezil autoradiography of porcine tissues and hematoxylin and eosin–stained slides for comparison. Right column shows nonspecific binding. (A) Stomach. There is high binding in mucosa, compared with muscle layers (asterisk). (B) Pancreas. (C) Spleen. There is relative high binding in lymphoid splenic nodules, whereas most red blood cells had been removed from sinusoids by buffer before incubation. (D) Submandibular gland. (E) Myocardium.

obtain the input function, 45 manual blood samples were taken during each dynamic scan. Plasma and whole-blood radioactivity were measured in a well counter (Cobra II; Packard Instrument Co.) cross-calibrated to the tomograph. The fraction of untransformed ¹¹C-donepezil was measured by radio–high-performance liquid chromatography in extracts of plasma from samples taken at 2, 5, 10, 15, 20, 30, and 60 min after injection. List-mode–acquired PET data were divided into 36 frames, 12 × 10, 6 × 30, 5 × 60, 5 × 120, and 8 × 300 s, and reconstructed using a 3-dimensional iterative algorithm (3 iterations, 21 subsets) including resolution modeling (TrueX), attenuation correction, and 3-mm gaussian filtering. The final image resolution was about 4.5 mm in full width at half maximum. Blood data and dynamic PET data were decay-corrected to scan start.

Volumes of Interest (VOIs)

For the whole-body dosimetry calculation, VOIs were manually defined (PMOD Software) in organs with elevated accumulation of tracer relative to surrounding tissue. For the liver, spleen, and lumbar vertebral bone marrow, the tracer concentration was determined from a VOI covering a central section of the organ. For smaller organs and organs appearing with high contrast relative to background, we extracted the total activity using VOIs completely surrounding the organ.

For dynamic PET analyses, the VOIs were based on anatomic CT scans, using different approaches. In the liver and spleen, VOIs were defined in the parenchyma 1 cm from the outermost tissue border. The pancreas, kidney cortex, and left myocardial ventricle were delineated on 6 consecutive slices using a 10-mm brush size in PMOD. Salivary glands were segmented using the CT scans. The correct location of the VOIs was evaluated on all individual PET frames and adjusted if necessary to correct for motion. Finally, for the stomach and small intestine, 2 VOIs were defined (Fig. 1). One large PET VOI was drawn to include all PET signal from the relevant organ but with sufficient distance from neighboring hot organs to avoid spill-in effects. Another, smaller VOI was automatically derived by segmenting the CT scan, using the large PET VOI as the constraining search space. The CT scans were smoothed using a 2-mm, isotropic gaussian filter, and a cutoff threshold of −20 Hounsfield units was used to define the small intestine and stomach VOIs, respectively. Voxels that did not derive from these organs (e.g., vessels) were removed manually. The final time–activity curves in the stomach and small intestine were obtained by scaling the curve from the PET VOI to this smaller CT volume. This procedure was chosen to compensate for frame-by-frame organ movement due to peristalsis.

the first scan, the upper abdomen/lower chest region (including heart, liver, intestines, and stomach) was in the field of view. For the second scan, the head including salivary glands was in the field of view. Low-dose CT scans were obtained of both regions for attenuation and anatomic localization purposes. For the upper abdomen, the PET average injected dose of ¹¹C-donepezil was 406 ± 104 MBq (range, 205–524 MBq) and for the head scans, 436 ± 49 MBq (range, 356–525 MBq). One head scan failed because of technical difficulties. To
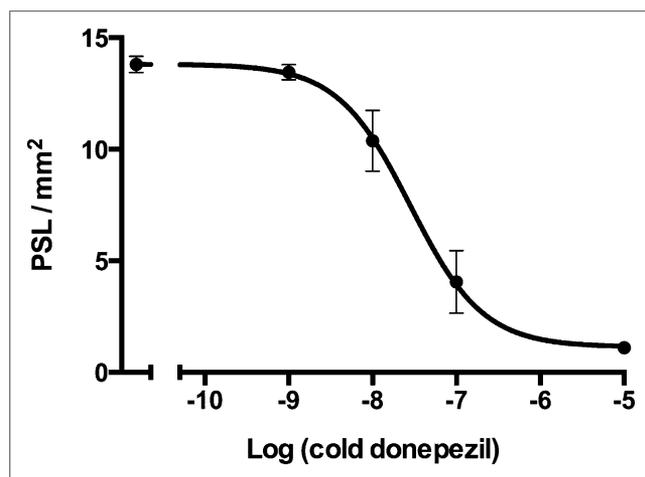

FIGURE 3. Representative inhibition curve from porcine submandibular gland. Mean ± SEM. PSL/mm² = photostimulated luminescence event per mm².

Kinetic Analyses

Dynamic PET time–activity curves were kinetically analyzed using arterial blood and plasma input functions and 3 nonlinear approaches: a reversible single-tissue-compartment model, an irreversible 2-tissue-compartment model, and a reversible 2-tissue-compartment model. Arterial plasma time–activity curves were used as the input function for the compartmental models and arterial blood time–activity curves to compute the blood volume. Goodness-of-fit was measured by the

TABLE 1
Autoradiography Data from Pig Tissue

Tissue	K_d (nM)	Nonspecific binding (%)
Stomach	17 (10–29)	3
Kidney	6	4
Pancreas	19 (2–161)	17
Spleen	25 (9–69)	6
Submandibular gland	28 (16–49)	6
Myocardium	30 (11–83)	16
Small intestines	39 (13–117)	17
Brain	18	14

Kidney and brain tissue values derived from only 1 pig. Data in parentheses are 95% confidence intervals.

Akaike score. Unconstrained fits of the 2-compartment models led to some negative parameter estimates, so those fits were repeated with a nonnegativity constraint. A 1-tissue-compartment model was found to be optimal; this model derives K_1 (mL mL^{-1} min^{-1}), the influx rate constant of the tracer from the plasma to the tissue compartment; k_2 (min^{-1}), the rate constant of transfer of tracer out of the tissue compartment; and V_b (mL mL^{-1}), the fractional blood volume in the tissue from the time–activity curves. We report estimates of total distribution volume ($V_d = K_1/k_2 + V_b$). Standardized uptake values (SUVs) were calculated on the basis of body weight—that is, SUV = concentration [kBq/mL] × (body weight [g]/injected dose [kBq]).

Infection Imaging

To investigate the possible uptake of ^{11}C-donepezil by infected tissue we obtained a 60-min dynamic ^{11}C-donepezil PET scan of a single female pig (Danish Landrace, 40 kg). Three weeks before PET, the pig had undergone experimental, abdominal surgery in another research protocol and abscesses had been observed. Bacteriologic characterization was performed on pus from 1 abscess. Before the PET scan, the pig was prepared and anesthetized as described previously (13). Permission for the PET scan was given by the Danish Animal Experiments Inspectorate. VOIs were placed over the abscesses to extract time–activity curves.
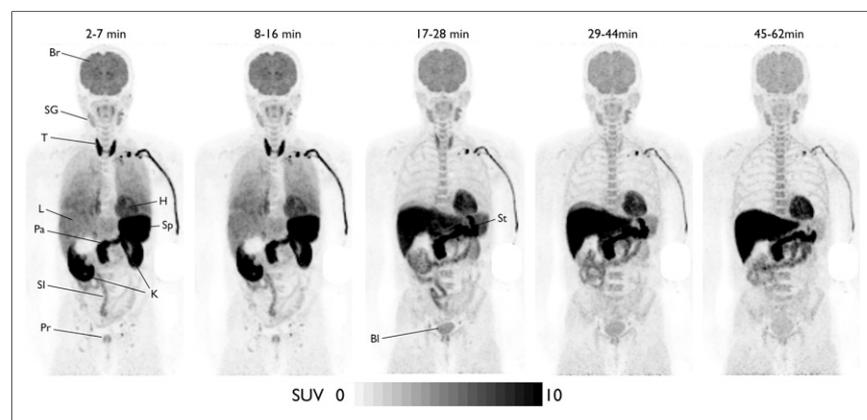
RESULTS

The radiopharmaceutical ^{11}C-donepezil was produced with high radiochemical yields, 2–2.5 GBq (corresponding to 50%–60% conversion of the collected ^{11}C-methyliodide to ^{11}C-donepezil), and a radiochemical purity greater than 99%. The present synthesis method gave higher yields than previously published methods (10). The mean specific radioactivity of ^{11}C-donepezil was 100 GBq/μmol (range, 50–200 GBq/μmol), with a final content of donepezil less than 1 μg/mL. Individual batch productions of ^{11}C-donepezil showed no alterations in appearance, pH, or chemical or radiochemical purity at 1 h after end of synthesis.

In Vitro Autoradiography

Figure 2 displays ^{11}C-donepezil binding in 5 different porcine tissues. Representative self-competition study data are shown in Figure 3. Binding affinities were high—that is, K_d values were all in the low nanomolar range (6–39 nM) and nonspecific binding was low (Table 1).

Whole-Body PET and Radiation Dosimetry

Whole-body biodistribution during a 62-min PET scan is depicted in Figure 4.

Radiation doses to organs are summarized in Table 2. The pancreas, spleen, and liver received the highest doses. The effective dose was 5.2 μSv/MBq.

Blood Data and Metabolites

The plasma activity peaked shortly after injection, followed by a rapid decline and nearly complete extraction by 20 min. The fraction of unchanged parent ^{11}C-donepezil in plasma was greater than 90% at 60 min after injection in all subjects (12 scans total).

Kinetic Analyses

The myocardium, salivary glands, small intestine, and pancreas displayed slow washout (Fig. 5A). These organs attained a plateaulike phase from 30 to 60 min after injection. The liver exhibited a continuously accumulating curve, whereas the kidney and spleen displayed rapid washout kinetics (Fig. 5B). The stomach showed an initial steep accumulation profile, followed by a highly variable washout among subjects (Supplemental Fig. 1). Prostate and thyroid data were available from only 1 subject (the whole-body dosimetry scan) and displayed slow and fast washout kinetics, respectively (Supplemental Fig. 1).

In the kinetic analyses using the 2-tissue-compartment models, the parameter estimates showed dependence on initial starting parameters and often led to nonphysiologic and even negative parameter estimates, whereas the 1-tissue-compartment model produced robust unconstrained fits. Furthermore, the 1-tissue-compartment model produced the lowest Akaike score in 56% of the fits (36% for the reversible 2-tissue-compartment model and 8% for the irreversible 2-tissue-compartment model). Thus, the reversible 1-tissue-compartment model was preferred on the basis of robustness of fits and Akaike scores. Table 3 displays mean SUV and K_d values from the 1-tissue-compartment reversible model. A linear correlation was seen between SUVs

FIGURE 4. Whole-body PET images of ^{11}C-donepezil in healthy volunteer. Bl = bladder; Br = brain; H = heart; K = kidney; L = lung; Pa = pancreas; Pr = prostate; SG = submandibular gland; SI = small intestines; Sp = spleen; St = stomach; T = thyroid.

TABLE 2
Human ^{11}C-Donepezil Dosimetry Estimates

Target organ	Dose (μSv/MBq)
Adrenals	14.6
Brain	8.0
Breasts	1.5
Gallbladder	5.4
Lower large intestine	2.0
Small intestine	8.4
Stomach	5.9
Upper large intestine	3.1
Heart	10.2
Kidneys	16.7
Liver	26.6
Lungs	2.3
Muscle	1.8
Ovaries	2.3
Pancreas	27.1
Red marrow	4.0
Skin	1.4
Spleen	22.1
Testes	1.3
Thymus	1.8
Thyroid	11.4
Urinary bladder	2.7
Uterus	2.2
Effective dose	5.2

obtained from the final PET frame and the V_d values derived from the 1-tissue-compartment model (Fig. 6).

Infection

Bacterial abscesses (nonhemolytic streptococci and Enterobacteriaceae) in an infected pig displayed high wall uptake (maximum SUV, 7.8 at 60 min) and slow washout kinetics (Fig. 7).

DISCUSSION

To our knowledge, this is the first human PET study to explore imaging of acetylcholinesterase density in peripheral organs. Tracer doses (<10 μg) of ^{11}C-donepezil were safe, and we observed no symptoms or adverse effects. Preliminary dosimetry calculations demonstrated that 500 MBq of ^{11}C-donepezil yield an effective dose of 2.6 mSv. In comparison, a 370-MBq clinical ^{18}F-FDG PET scan yields a dose of 7.4 mSv. This radioactive dose allows repeated ^{11}C-donepezil PET scans in single subjects or the use of ^{11}C-donepezil as a part of multitracer PET studies without excessive radiation exposure. One possible source of error in the dosimetry estimates is posed by the stomach and intestines doses. In the current OLINDA software package, only values of intraluminal stomach/intestinal content can be entered. However, based on the porcine autoradiography (Fig. 2A), ^{11}C-donepezil displays high binding to mucosa. Thus, it is possible that the stomach and intestine organ doses were underestimated by the current calculation.

[11]C-donepezil is peripherally metabolized slowly. A previous study of Japanese subjects reported 91% unchanged ligand at 30 min (10). The authors demonstrated that metabolite correction could be omitted in ^{11}C-donepezil brain studies with only minor impact on the kinetic parameter estimates. In the present Caucasian study population, peripheral metabolism was even slower. The parent fraction was greater than 90% at 60 min in all subjects, perhaps reflecting different rates of donepezil metabolism in Japanese and Caucasian subjects. Thus, metabolite correction is most likely unnecessary in the context of a 60-min ^{11}C-donepezil PET study.

Autoradiography experiments of porcine tissues confirmed specific binding of ^{11}C-donepezil to brain tissue and 7 different peripheral organs. Nonspecific binding was low (<17%), and binding affinities were high. K_d values were in the low nanomolar range, in accordance with literature K_d values for acetylcholinesterase in brain tissue (6 nM) (9). Some tissue inhomogeneity was observed. In the small intestine and stomach (Fig. 2), intense signal was seen in the mucosa, which contains the submucosal plexus. In comparison, only moderate signal intensity was seen in the muscle layers, containing the myenteric plexus. A large fraction of enteric neurons are cholinergic (14), and the present study cannot quantify the relative magnitude of the PET signal coming from vagal innervation vis-à-vis cholinergic enteric neurons.

In the spleen, specific signal was seen in the lymphoid nodules, probably reflecting binding to immune cells (5). The red blood cells were mostly removed from the splenic sinusoids by the buffer before incubation. Had this not been the case, we would probably have seen specific binding to red blood cells, which are known to be rich in acetylcholinesterase. A more homogeneous signal was seen throughout the kidney cortex, pancreas, and submandibular gland. These organs are all richly innervated by parasympathetic nerve fibers, making it likely that a large fraction of the PET signal corresponds to parasympathetic innervation. Final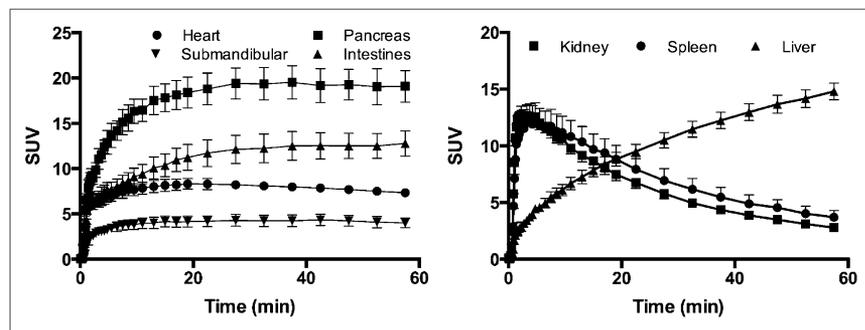ly, homogeneous and displaceable signal was seen in the left ventricle of the heart. Although the heart receives parasympathetic innervation, the relative distribution of this innervation to different parts of the heart is unclear. Previous studies in pigs and humans (15,16) demonstrated a dense network of acetylcholinesterase-rich nerve fibers in the endo-, myo-, and epicardium, but some of these fibers probably originate from intrinsic cardiac ganglia. More recently, it has been shown that cardiomyocytes synthesize and secrete acetylcholine to support parasympathetic cardiac innervation (17), although no specific staining for acetylcholinesterase

FIGURE 5. Time–SUV curves (mean ± SEM) of ^{11}C-donepezil in various organs (n = 6).

TABLE 3
SUV and V_d Values in 7 Organs (Human)

Region	SUV Mean ± SD	SUV COV (%)	V_d Mean ± SD	V_d COV (%)
Parotid	2.3 ± 0.5	21	18.0 ± 3.3	19
Submandibular	3.9 ± 1.1	30	22.1 ± 5.0	22
Spleen	3.7 ± 1.4	38	21.4 ± 7.6	35
Stomach	4.8 ± 1.2	25	26.6 ± 11.5	43
Heart	7.4 ± 0.8	11	46.8 ± 7.8	17
Intestine	11.7 ± 2.4	21	103.9 ± 19.5	19
Pancreas	19.1 ± 4.2	22	189.8 ± 103.9	55

COV = coefficient of variation.

was performed in these studies. In summary, future studies are needed to clarify whether the intense cardiac ^{11}C-donepezil signal reflects parasympathetic innervation.

Varying kinetic behavior of ^{11}C-donepezil was observed in different organs. An especially intriguing finding was the slow washout and plateaulike phase observed 30–60 min after injection from salivary glands, heart, pancreas, intestine, and prostate. We found a clear correlation between SUVs and V_d estimates from the 1-tissue-compartment model (Fig. 6). However, uptake in high-V_d organs, such as the small intestine, behaved almost irreversibly, leading to high V_d estimates. Apart from these few outliers, there was an almost linear relation between SUVs and V_d. Taken together,

these observations suggest that arterial sampling may be omitted altogether and that SUVs obtained from a whole-body ^{11}C-donepezil PET study performed 40–60 min after injection may allow valid quantitation. Of note, ^{11}C-donepezil accumulates irreversibly in the liver and is subsequently metabolized. Therefore, liver acetylcholinesterase density cannot be meaningfully estimated using this tracer.

We suggest that ^{11}C-donepezil may be able to quantify parasympathetic denervation in disorders such as Parkinson disease. Acetylcholinesterase is produced in the perikaryon of cholinergic neurons and transported to dendrites and axons, where it is inserted into membranes as an ectoenzyme (18). Thus, damage to vagal efferents would be expected to decrease vagus-derived acetylcholinesterase in the gastrointestinal tract. A previous study demonstrated a 40%–50% acetylcholinesterase activity decrease in the duodenum and colon of guinea pigs after vagotomy (2). However, we must emphasize that acetylcholinesterase is not a specific marker for vagal cholinergic parasympathetic innervation. An abundance of enteric neurons are cholinergic and express acetylcholinesterase (14).

We demonstrated ^{11}C-donepezil uptake in bacterial abscesses. Tracer washout was slow, and the SUVs were quite high. To our knowledge, this is the first in vivo PET demonstration of cholinergic signal processing in infections, suggesting that ^{11}C-donepezil could be a valuable tool for elucidating the immune modulatory effects of acetylcholinesterase in patients with infectious and rheumatologic diseases.

This study has limitations. Human tissue would have been preferable for the autoradiography studies, because species-specific differences in ^{11}C-donepezil binding affinity may exist. In the human PET studies, we obtained only 60-min dynamic PET scans and it is likely that a steady state was not completely attained. However, the short half-life of ^{11}C-labeled compounds (20.3 min) impacts on image quality when using more prolonged scan times. Considering that ^{11}C-donepezil extraction from the plasma is nearly complete at 20–30 min, and that tissue time–activity curves had reached the plateau- or declining (washout) phase at 40 min, it is feasible to obtain dynamic (0–60 min) or static (40–60 min) PET scans with ^{11}C-donepezil. We did not perform pharmacologic displacement in the human PET studies. Thus, our V_d estimates constitute the total distribution volume not specific distribution volume. However, our porcine autoradiography studies demonstrated nonspecific binding of only 4%–17% in the investigated organs. Also, a previous ^{11}C-donepezil study of patients with Alzheimer disease showed that brain V_d values decreased by 62% subsequent to pharmacologic treatment with donepezil (5 mg), suggesting that ^{11}C-donepezil is highly displaceable (7). Future human ^{11}C-donepezil studies with displacement could identify possible reference regions for noninvasive quantification of acetylcholinesterase density.
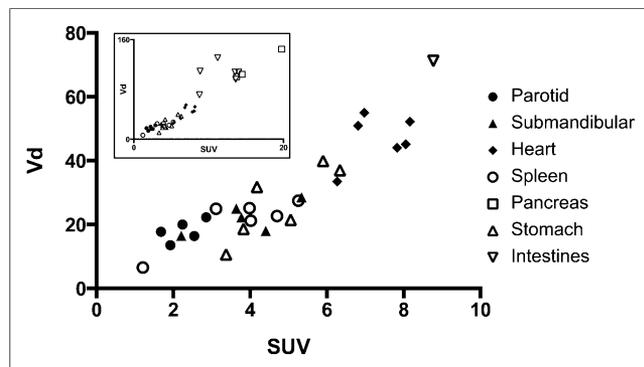

FIGURE 6. Correlations between SUVs in last PET frame (55–60 min) and V_d values derived from 1-tissue-compartment reversible model. Inset includes values from high-binding organs (intestines and pancreas).
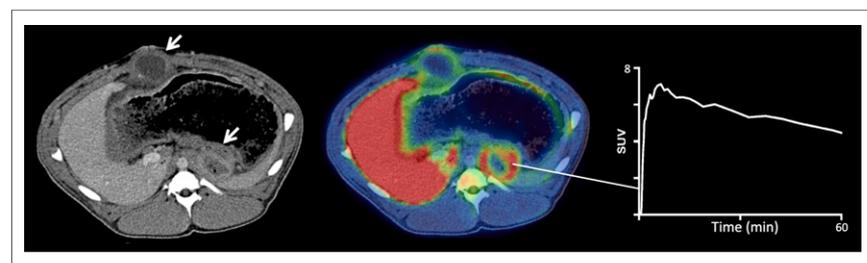

FIGURE 7. High ^{11}C-donepezil uptake and slow washout kinetics were seen in 2 abscesses of pig (arrows). PET image displays final frame (55–60 min).

CONCLUSION

We demonstrated that ^{11}C-donepezil PET is feasible for imaging acetylcholinesterase densities in peripheral organs. The ligand binds specifically with high affinity to a range of tissue types, and slow metabolization obviates the need for radiometabolite correction. We demonstrated a linear relationship between V_d values and simple SUVs at 60 min in most organs, suggesting

for these that static PET imaging without arterial blood sampling may be valid. Bacterial abscesses in an infected pig displayed high ^{11}C-donepezil binding. We propose that ^{11}C-donepezil PET imaging may be able to visualize parasympathetic denervation but also nonneuronal cholinergic mechanisms in infections.

DISCLOSURE

REFERENCES

1. Bohnen NI, Muller ML, Kotagal V, et al. Heterogeneity of cholinergic denervation in Parkinson's disease without dementia. *J Cereb Blood Flow Metab.* 2012;32:1609–1617.
2. Schmid W, van der Zypen E, Keller H. Die wirkung einer subtotalen vagotomie auf den plexus myentericus (Auerbach) verschiedener darmabschnitte. *Acta Anat (Basel).* 1979;104:36–51.
3. Pauza DH, Saburkina I, Rysevaite K, et al. Neuroanatomy of the murine cardiac conduction system: a combined stereomicroscopic and fluorescence immunohistochemical study. *Auton Neurosci.* 2013;176:32–47.
4. Cersosimo MG, Benarroch EE. Pathological correlates of gastrointestinal dysfunction in Parkinson's disease. *Neurobiol Dis.* 2012;46:559–564.
5. Kawashima K, Fujii T, Moriwaki Y, Misawa H. Critical roles of acetylcholine and the muscarinic and nicotinic acetylcholine receptors in the regulation of immune function. *Life Sci.* 2012;91:1027–1032.
6. Kikuchi T, Okamura T, Zhang MR, Irie T. PET probes for imaging brain acetylcholinesterase. *J Labelled Comp Radiopharm.* 2013;56:172–179.
7. Okamura N, Funaki Y, Tashiro M, et al. In vivo visualization of donepezil binding in the brain of patients with Alzheimer's disease. *Br J Clin Pharmacol.* 2008;65:472–479.
8. Hiraoka K, Okamura N, Funaki Y, et al. Cholinergic deficit and response to donepezil therapy in Parkinson's disease with dementia. *Eur Neurol.* 2012;68:137–143.
9. Wilkinson DG. The pharmacology of donepezil: a new treatment of Alzheimer's disease. *Expert Opin Pharmacother.* 1999;1:121–135.
10. Hiraoka K, Okamura N, Funaki Y, et al. Quantitative analysis of donepezil binding to acetylcholinesterase using positron emission tomography and [5-^{11}C-methoxy] donepezil. *Neuroimage.* 2009;46:616–623.
11. Cheng Y, Prusoff WH. Relationship between the inhibition constant (K1) and the concentration of inhibitor which causes 50 per cent inhibition (I50) of an enzymatic reaction. *Biochem Pharmacol.* 1973;22:3099–3108.
12. Stabin MG, Sparks RB, Crowe E. OLINDA/EXM: the second-generation personal computer software for internal dose assessment in nuclear medicine. *J Nucl Med.* 2005;46:1023–1027.
13. Ettrup KS, Glud AN, Orlowski D, et al. Basic surgical techniques in the Gottingen minipig: intubation, bladder catheterization, femoral vessel catheterization, and transcardial perfusion. *J Vis Exp.* 2011;52:2652.
14. Anlauf M, Schafer MK, Eiden L, Weihe E. Chemical coding of the human gastrointestinal nervous system: cholinergic, VIPergic, and catecholaminergic phenotypes. *J Comp Neurol.* 2003;459:90–111.
15. Crick SJ, Anderson RH, Ho SY, Sheppard MN. Localisation and quantitation of autonomic innervation in the porcine heart II: endocardium, myocardium and epicardium. *J Anat.* 1999;195:359–373.
16. Marron K, Wharton J, Sheppard MN, et al. Human endocardial innervation and its relationship to the endothelium: an immunohistochemical, histochemical, and quantitative study. *Cardiovasc Res.* 1994;28:1490–1499.
17. Roy A, Fields WC, Rocha-Resende C, et al. Cardiomyocyte-secreted acetylcholine is required for maintenance of homeostasis in the heart. *FASEB J.* 2013;27:5072–5082.
18. Giacobini E. *Cholinesterases and Cholinesterase Inhibitors.* London, U.K.: Martin Dunitz Ltd.; 2000.